TUDelft

Delft University of Technology

The effect of temperature on fatigue strength of poly(ether-imide)/multiwalled carbon nanotube/carbon fibers composites for aeronautical application

Santos, Luis F.P.; Ribeiro, Bruno; Hein, Luis R.O.; Alderliesten, René; Zarouchas, Dimitrios; Botelho, Edson C.; Costa, Michelle L.

Important note
To cite this publication, please use the final published version (if applicable).
Please check the document version above.

ARTICLE

Applied Polymer WILEY

The effect of temperature on fatigue strength of poly(ether-imide)/multiwalled carbon nanotube/carbon fibers composites for aeronautical application

Luis F. P. Santos[1] 🟢 | Bruno Ribeiro[2] | Luis R. O. Hein[1] | René Alderliesten[3] |
Dimitrios Zarouchas[3] | Edson C. Botelho[1] | Michelle L. Costa[1]

[1]Materials and Technology Department,
School of Engineering, São Paulo State
University (UNESP), Guaratinguetá,
Brazil

[2]Institute of Science and Technology,
Federal University of São Paulo
(UNIFESP), São José dos Campos, Brazil

[3]Structural Integrity & Composites,
Aerospace Engineering, Delft University
of Technology (TU-DELFT), Delft, The
Netherlands

Correspondence
Luis F. P. Santos, Materials and
Technology Department, School of
Engineering, São Paulo State University
(UNESP), Guaratinguetá, Brazil.
Email: luis.santos@unesp.br

Abstract

This work concerns the fatigue behavior at three different temperature conditions (−40, 20, and 80°C) and the addition of multiwalled carbon nanotube (MWCNT) into a carbon-fiber reinforced poly(ether-imide) composite. The incorporation of MWCNT into the composite increased the tensile strength and Young's modulus by up 5 and 2%, respectively. At low temperature, the incorporation of the nanoparticles improved the fatigue strength of the laminates by 15%. The shear strength results obtained by interlaminar shear strength and compression shear test tests have shown an increase of about 16 and 58%, respectively, by the introduction of nanotubes into the laminates. Fractographic observations revealed that the surface of carbon nanotube laminate (PEI/MWCNT/CF) presented a ductile behavior, and differences in the fracture aspects of the material compared to the traditional PEI/CF laminate have been observed.

KEYWORDS

composites, fullerenes, graphene, mechanical properties, microscopy, nanotubes

1 | INTRODUCTION

The advances in nanotechnology and the constant requests for better quality, lower cost, and unique properties have led to the development of new materials with exceptional properties in order to promote higher efficiency and lower energy consumption for aircrafts. One such improvement, the incorporation of nanoscale particles into the polymer matrix, has been subject to study over the last two decades. Multiple studies report that nanoscale particles can promote improvements in the performance of the material, such as thermal, mechanical, electrical, and magnetic features.[1–6] Carbon nanotubes (CNT), one of the most important materials employed in the production of nanostructured composites, were discovered by Sumio Iijima in 1991.[7] The CNT can be defined as a perfect sheet of graphene rolled into a cylinder, that is, a network of sp^2 carbon atoms (the hybridization of carbon when it has a double bond and two single bonds or one π bond and three σ bond) in

the hexagonal form, showing a length around micrometers (μm) and diameter of nanometers (nm).[7,8] The use of CNT as a nanoreinforcement in polymeric systems has increased over the years due to their high-aspect ratio and exceptional mechanical features that are intrinsic to the sp^2–sp^2 covalent bonds (covalent bonds between the layers of carbon atoms sp^2). These covalent bonds (sp^2–sp^2) promote excellent mechanical properties to this material, such as high-elastic modulus (200–5,000 GPa), high-tensile strength (200 GPa) and high electrical (10^3–10^5 S/cm) and thermal conductivities (2,000 W m^{-1} K^{-1}).[1,8–10]

The main challenge associated with the development of CNT-reinforced composites is the agglomeration of nanoparticles during material processing. This fact may be associated with the high-aspect ratio and the chemical nature of the nanoparticles, as both influence the molecular dynamics of the polymer.[11,12] Agglomeration of the CNT generates nonhomogeneous composites, which may result in the deterioration of the final properties of the material.[13] Therefore, a major challenge in the development of CNT/polymer composites consists of obtaining a satisfactory dispersion of the filler in the polymer matrix maximizing the properties of the final product. The functionalization process appears to prevent the CNT agglomeration, improving the interfacial adhesion between the polymer matrix and the nanoparticles.[14] The addition of functional groups to the nanotube walls, such as the carboxyl group (COOH), changes the CNT behavior from hydrophobic to hydrophilic, enhancing the interface between the tubes and the polymer matrix.[8,15] According to Yang,[16] the incorporation of MWCNT-COOH into epoxy improved both the impact strength and bending properties, as well as an increase in the thermal conductivity of the composites. Also, Francisco[17] observed an increase in hardness for functionalized-CNT/epoxy systems.

The use of carbon fiber-reinforced polymer composites (CFRP) has increased over the last decades.[18] Thermoplastic laminates have gained prominence in the market, due to their easier processability, superior impact toughness, high-damage tolerance, and higher temperatures of service compared to thermoset structures.[19–22] Also, thermoplastics matrices exhibit a near-infinite shelf life at room temperature. This compares quite favorably to the shelf life of fewer than 6 months in refrigerated storage for typical prepreg thermoset materials.[21,23] There is a wide range of thermoplastic materials used in advanced composites structures for the aerospace industry. The most frequently seen are poly(ether-imide) (PEI), poly (phenylene sulfide) (PPS), poly(ether ketone ketone) (PEKK), and poly(ether ether ketone) PEEK.[19]

PEI is a high-performance thermoplastic material, which has several applications in aeronautical, electronics, automotive, and medical areas. The polymer matrix shows the amorphous structure with a glass transition temperature of around 217°C, high-mechanical strength, high stiffness, easy processability, and good flame resistance with low content of smoke. Such properties are mostly due to the presence of aromatic imides and ether units in its polymer chain.[24–26] The aforementioned characteristics make this polymer attractive for applications in aircraft interior segments, and also the wing ribs, main landing gear door, and flap ribs.

Thermoplastics laminates are constantly exposed to different loading conditions such as high-temperature range and moisture, affecting the service life of materials.[27–29] Among several failure mechanisms reported for CFRP, the most common are failures due to fatigue and interlaminar fracture, known as delamination.[27,28,30,31] Fatigue damage results in a change of strength, stiffness, and other mechanical properties of composite materials[32] and it is estimated to cause approximately 60% of total aircraft component failures.[33] The mechanisms of damage in composites laminates can be demonstrated in three steps: the first stage (I) is explained by a reduction of the material's stiffness due to the formation of microcracks in the material; the second stage (II) is characterized by microcracks nucleation and minor levels of damages; the third stage (III) is governed by the failure occasioned due to catastrophic propagation of microcracks.

Therefore, crack nucleation increases as a function of stress intensity that is directly linked to topography (surfaces and interfaces), voids, inclusion, and defects. Topography aspects, like roughness, provide information on the intensity and density of potential stress concentrators and the opposite, smooth surface, suggests that the material needs more time for crack nucleation.[34,35]

Interlaminar fracture (delamination) is an issue that limits the application of composites laminates, as it promotes a significant reduction of structural stiffness, usually without external signs of damage, resulting in a catastrophic failure.[36] The delamination can be explained by the low interlaminar shear strengths between fiber and matrix components, and by the brittle behavior in the case of thermoset systems. Also, the delamination between the composite layers is often initiated by bonding imperfections, and by a weak fiber/matrix interface.[37] The interlaminar strength for polymer composites depends on the polymeric matrix characteristics and the interface between the components. Also, these two aspects are an important source of weakness in the material and shear stresses.[38] One of the solutions to improve the interlaminar properties of the laminates

comprises the addition of nanoparticles to enhance the matrix hardness, promoting an increase in fracture properties, and extending the life of the material.[37–39]

In addition to various load conditions that a CFRP may be subjected to, another aspect that must be considered is the environmental condition the laminate is exposed to. During their lifetime, composite materials are subjected to severe environmental conditions, such as hygrothermal exposure and ultraviolet radiation. Both conditions can weaken the matrix properties, as well as the interfacial adhesion between polymer and fibers, revealing irreversible changes in the material.[40,41] The ultraviolet radiation promotes the degradation by photo and thermooxidative reactions, whereas in hygrothermal aging the moisture is introduced preferential in the matrix and/or fiber–matrix interface since the carbon fibers do not absorb moisture. Besides, microcracks and microvoids can be introduced into the laminate by the diffusion of water molecules. Water interacts with both polymer matrix and fibers, especially in the interfacial zone, causing the degradation of the properties of the composites.[40,42–44]

In this article, the influence of the incorporation of multiwalled carbon nanotubes (MWCNTs) on the fatigue strength of the PEI/CF composite submitted to low ($-40°C$), room ($20°C$), and high temperature ($80°C$) was evaluated. Also, the effect of carbon nanotubes on the interlaminar fracture strength through ILSS and CST exposed to hygrothermal aging and ultraviolet radiation was investigated. The mechanical tests were complemented with a fractographic analysis to evaluate the failure modes of the materials.

2 | MATERIALS AND METHODS

2.1 | Materials

Poly(ether-imide) was supplied by a Saudi company Sabic's Innovative Plastics under the commercial name ULTEM 1010 and has the following properties: density of 1.28 g/cm^3 and glass transition temperature (T_g) of $217°C$. The carbon fiber weave used for manufacturing the laminates were supplied by the American company Hexcel Composites, containing 3,000 cable monofilaments, a plain weave arrangement, a specific mass of 1.77 g/cm^3, without sizing treatment and a thickness of about 0.17 mm. MWCNTs were supplied by Cheap Tubes from United States with a wall diameter of 8–15 nm, a length between 10 and 50 μm, and $d_{25°C} = 2.1$ g/cm^3. The MWCNT were acid-treated by the manufacturer, with the incorporation of a carboxyl group (COOH) into the nanotube walls by using a mixture of inorganic acids (sulfuric

and nitric). The solvent used during the preparation of the composites was methylene chloride (Neon from Brazil), and Triton X-100 surfactant (Labsynth from Brazil) was employed to improve the dispersion of the nanoparticles in the composite.

2.2 | Composite processing

The laminates used in this work (PEI/CF and PEI/MWCNT/CF) were prepared in two steps. A neat PEI film with thickness around 0.1 mm, was obtained by solution mixing process considered the most common technique for processing nanostructured polymer composites.[45] First, 10 g of the polymer (pellets) was dissolved in 250 ml of methylene chloride under stirring for 30 min. Subsequently, the solution was transferred to an aluminum mold with dimensions of (30×30) cm and taken to a vacuum oven (Vacucell, model VUK/VU 55) at $40°C$ for 3 hr to dry the solvent. It is worth mentioning that the temperature of $40°C$ was chosen due to it is close to the boiling temperature of the solvent. The PEI/MWCNT film was prepared in the same way, by adding 0.1 g of MWCNT, which corresponds to 1 wt% based on polymer mass. Triton X-100 (0.5 g) surfactant was dispersed in 50 ml of methylene chloride for 30 min with the aid of an ultrasonic tip (Sonics & Materials, model VC 750). In parallel, 10 g of PEI was dispersed in 200 ml methylene chloride for 30 min under magnetic stirring. Subsequently, the solutions were mixed and taken to the ultrasonic tip for a further 40 min dispersion. The PEI/MWCNT, methylene chloride, and Triton X-100 solution was placed in an aluminum mold with dimensions (30×30) cm and dried at $40°C$ for 3 hr for solvent removal. The parameters used during the processing of the films on the ultrasonic tip were 25% amplitude and a pulse of 10 s on and 5 s off. Triton X-100 surfactant was used to assist in the dispersion stability of the carbon nanotubes. The percentage of 1 wt% of MWCNT used in this work was chosen based on some studies in the literature,[3,46] which obtained electrical percolation, better mechanical properties, increased thermal conductivity, and stiffness with the addition of only 1% of MWCNT.

After preparing the polymeric film, the laminates were processed by stacking 16 layers of PEI/MWCNT films and 12 layers of plain weave carbon fiber fabric $(0°/90°)$. It is worth mentioning that two polymer layers are inserted after the third, sixth, and ninth layers of carbon fiber to guarantee the full percolation of the matrix through the fibers. The laminate was manufactured by hot compression molding (Carver hydraulic press, model CMV100H-15-X) at $320°C$ for 30 min with an applied

pressure of 1.5 MPa. Control samples (PEI/CF) have been prepared in the same way.

The volumetric fiber fraction of the composites was 60% and the void content was around 1.5%. This information was obtained from the acid digestion procedure according to ASTM D3171. All the processing conditions are described in our previous paper.[47]

2.3 | Tensile test

The tensile test was performed according to ASTM D303 and aimed to evaluate the influence of the addition of MWCNT on PEI/CF laminate's tensile strength and Young's modulus (E). The tensile test was performed at Delft University Technology (The Netherlands) using a ZWICK universal mechanical testing machine model Z250. The equipment presented accuracy and position repeatability of ± 2 μm. The test was performed at room (20°C), low (−40°C), and high (80°C) temperatures. These temperatures were measured using a thermocouple placed in the central region of the sample and a constant speed of 2 mm/min with a 250 kN load cell and extensometer were applied. Six specimens for the room temperature condition and two specimens for each low and high temperatures were employed. The dimensions of the samples were (250 × 25.415 × 2.78) mm for PEI/CF and (250 × 25.158 × 2.41) mm.

According to ASTM D303 the maximum tensile strength can be calculated as follows:

$$F^{tu} = \frac{P_{max}}{A} \qquad (1)$$

The Young modulus can be described as:

$$E = \frac{\Delta_\sigma}{\Delta_\varepsilon} \qquad (2)$$
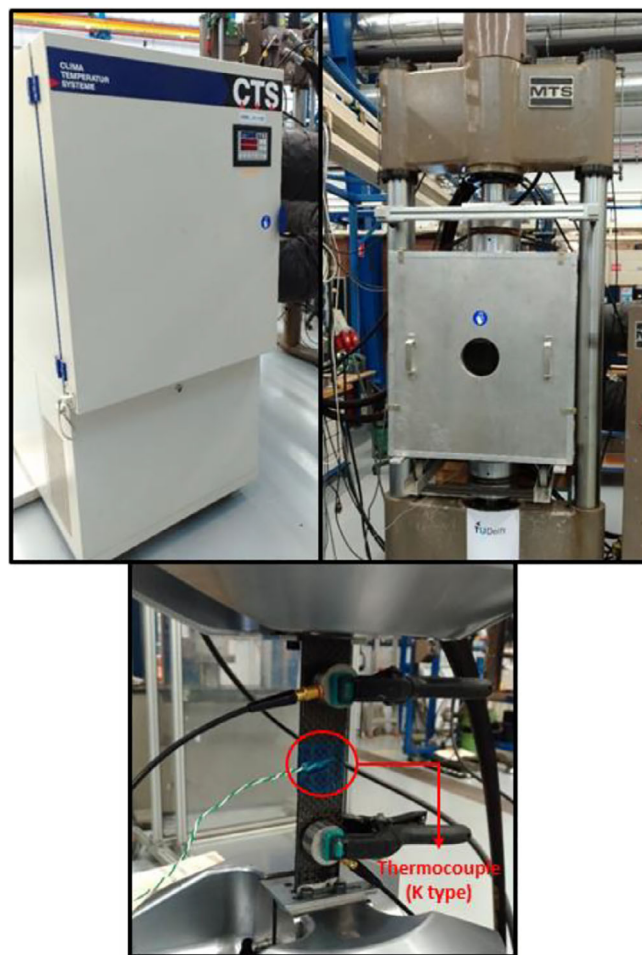
2.4 | Fatigue test

The fatigue test was performed according to ASTM D3479 in tensile-tensile mode. The studied material is meant to be applied in the aeronautical sector, therefore, the test temperatures were derived from the aircraft flight envelope, that is, the tests were carried out at low (−40°C), room (20°C), and high (80°C) temperatures. The parameters used for these tests were: load cell of 100 kN, a load ratio of 0.1, a frequency of 5 Hz and 65% of the maximum tension obtained in the tensile test. The test was performed on a universal test machine (MTS

100 kN) at Delft University Technology (The Netherlands). For the tests performed at low and high temperatures, a home-build aluminum temperature chamber was used, and connected to another chamber to promote the heating of the samples, as presented in Figure 1. Also, liquid nitrogen was used to reach low temperatures (−40°C) inside the chamber.

2.5 | Environmental aging

Before testing, the specimens were conditioned in a drying process, in which they were first weighed and placed in a vacuum oven at 80°C. Every 12 hr the mass of samples with dimensions (40 × 40 × 2.5) mm was measured. Only after weight stabilization, the specimens were submitted to the respective tests.

The hygrothermal aging was performed according to ASTM D5229 in a computerized climate chamber (Marconi-Brazilian brand), where the specimens were exposed to 90% relative humidity at 80°C for 8 weeks.

FIGURE 1 Configuration used to perform the fatigue test [Color figure can be viewed at wileyonlinelibrary.com]

The mass of samples was measured once a week, and only after their stabilization (8 weeks), the test was terminated. The ultraviolet radiation with a condensation test was carried out according to ASTM G 154 standard (Q-Lab). The samples were exposed to 1,200 hr in alternate cycles of 8 hr at 60°C under ultraviolet radiation, and for 4 hr at 50°C under water condensation. The UV radiation exposure was performed by UV-A lamps with 340 nm wavelength and 0.76 W/m^2 intensity.

2.6 | Interlaminar shear strength (ILSS)

Interlaminar shear strength tests were carried out according to ASTM D2344/D2344M-16. A mechanical test machine (Shimatzu, autograph AG-X series) was used to perform the mechanical analyses according to the following parameters: speed of 1.0 mm/min and a load cell of 10 kN. Ten specimens for each condition were tested with dimensions (18 × 6 × 3) mm. The short-beam (F^{sbs}) strength was calculated according to,

$$F^{sbs} = \frac{0.75P}{bh} \qquad (3)$$

where P is the maximum load obtained during the test, b is the specimen width, and h is the specimen thickness.

2.7 | Compression shear test (CST)

The compression shear test was developed at the Institute of Polymer Research, in Dresden (Germany) by the researchers Schneider, Lauke, and Becker.[48] The focus of this test is to promote a direct shear loading along the interlaminar interface, to force the specimen to fail in pure shear. The loading distribution is almost uniform along the thickness with two peaks close to the edges of the loading surface. The parameters applied to perform this test were as follows: five specimens for each condition with dimensions of (10 × 10 × 3) mm, a speed test of 0.25 mm/min and a 10 kN load cell. The apparent interlaminar shear stress was calculated according to:

$$\sigma_{app} = \frac{P_{eff}}{(l \times b)} \qquad (4)$$

$$P_{eff} = \frac{P_{tot} \times z}{(R_d + d_i)} \qquad (5)$$

where σ_{app} is the interlaminar shear stress (MPa), P_{eff} is the effective load (Kgf), P_{tot} is the load applied (Kgf), z is the distance between the pivot and movable arm (mm), R_d is the radius of movable arm (degrees), and d_i is the

half-width of the sample (mm) which is subjected to the compression force. Therefore, the Figure 2 shows the device used to perform this test.

2.8 | Morphological analyses

The morphological analyses were performed in two stages: in the first stage, the dispersion of carbon nanotubes in the polymeric matrix was evaluated, while in the second stage the morphological analysis of the fracture surface was performed after the mechanical tests. To evaluate the dispersion of carbon nanotubes into the polymer matrix, samples were obtained from the cross-section region of the PEI/MWCNT film, cleaned with a nitrogen jet, and covered with a gold layer to be subsequently evaluated by scanning electron microscopy (SEM-EVO LS-15) and also atomic force microscopy (AFM) was also performed using a Shimadzu microscope, model SPM-9600. The samples were fractured, cleaned with a jet of nitrogen and placed on the aluminum sample port. In the second step, after the mechanical tests, the samples were carefully cross-sectioned to protect the fracture surface from potential contamination and maintain their topology. The sanding and polishing steps have not been performed to avoid damage to the fracture surface. SEM was employed to evaluate the failure modes for tensile and fatigue tests. During this analysis back-scattered (BSE) signals were obtained using the Zeiss 4Q-BSD, a four-quadrant semiconductor detector, with an acceleration voltage of 12 kV for matrix characterization and 5 kV for fractographic analysis. Also, optical microscopy (Zeiss model Imager Z2m) was used to evaluate the fracture surface of the specimens submitted to CST and ILSS tests, once interlaminar fractures are best analyzed using optical microscopy through crack propagation analysis.
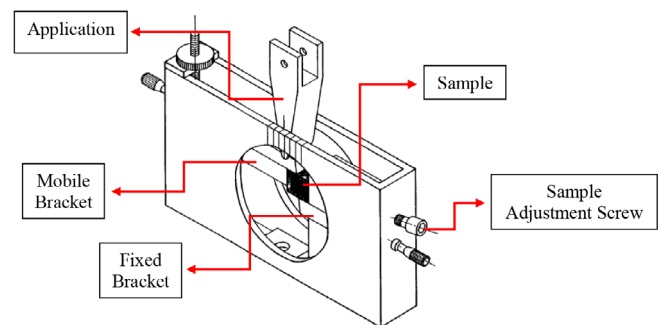
FIGURE 2 Device used for conducting the mechanical test of compression shear test (CST) [Color figure can be viewed at wileyonlinelibrary.com]

3 | RESULTS AND DISCUSSION

3.1 | Evaluation of multiwalled carbon nanotube dispersion

The morphology of PEI/MWCNT was evaluated by SEM and AFM as can be observed in Figure 3. Figure 3a shows the PEI/MWCNT film presented a certain homogeneity in its morphology, but clusters and agglomerates can be identified (red circle). This behavior can be associated with strong van der Walls interaction between the tubes.[13,46] The clusters observed in the micrographs were measured and their average size was around 154.5 $\pm$ 34.1 nm. Figure 3b presents structures like crystals, named here as pseudo-crystals. As previously mentioned in this work, the poly(ether-imide) matrix is an amorphous polymer, and thus no crystalline structures were expected. These pseudo-crystals, generated from the addition of MWCNTs, promoted a high degree of aggregation of the nanoparticles in the polymer matrix. This behavior ordered the polymeric chain, especially in soft and flexible areas of the matrix. These pseudo crystals changed the material morphology, acting mainly on the macroscopic properties of the material, especially on the mechanical properties.[49] Such aspects could be related to the covalent functionalization of the MWCNT from the addition of the carboxyl group and the noncovalent functionalization from the use of Triton X-100 surfactant that assists in obtaining homogeneous structures.

3.2 | Tensile strength tests

The tensile test was performed to obtain the maximum tensile strength, as well as the Young's Modulus of the prepared laminate since the data are useful for the fatigue analyses. Table 1 presents the tensile results of the studied samples.

The incorporation of MWCNT into the composite generated a small increase in tensile strength, from 611.8 MPa (43 kN) for PEI/CF to 642.7 MPa (39 kN) for PEI/MWCNT/CF, representing an enhancement of 5%. The Young's modulus (E) has shown an increase from 24.2 GPa (PEI/CF) to 24.7 GPa (PEI/MWCNT/CF), representing a small gain of 2% in elastic properties of the nanostructured composite. Also, the tensile strength of PEI/CF was close to those obtained in the literature for Carbon T300 3K reinforced PEI composite which have values between 656 and 673 MPa.[27] Taking into account the standard deviation obtained for the samples it is found that the increase of F^{tu} and E were not significant. This composite was taken as reference, once it contains the same polymer matrix with similar carbon fiber reinforcement.

The improvement in the mechanical behavior of composite materials subjected to tensile loading promoted by
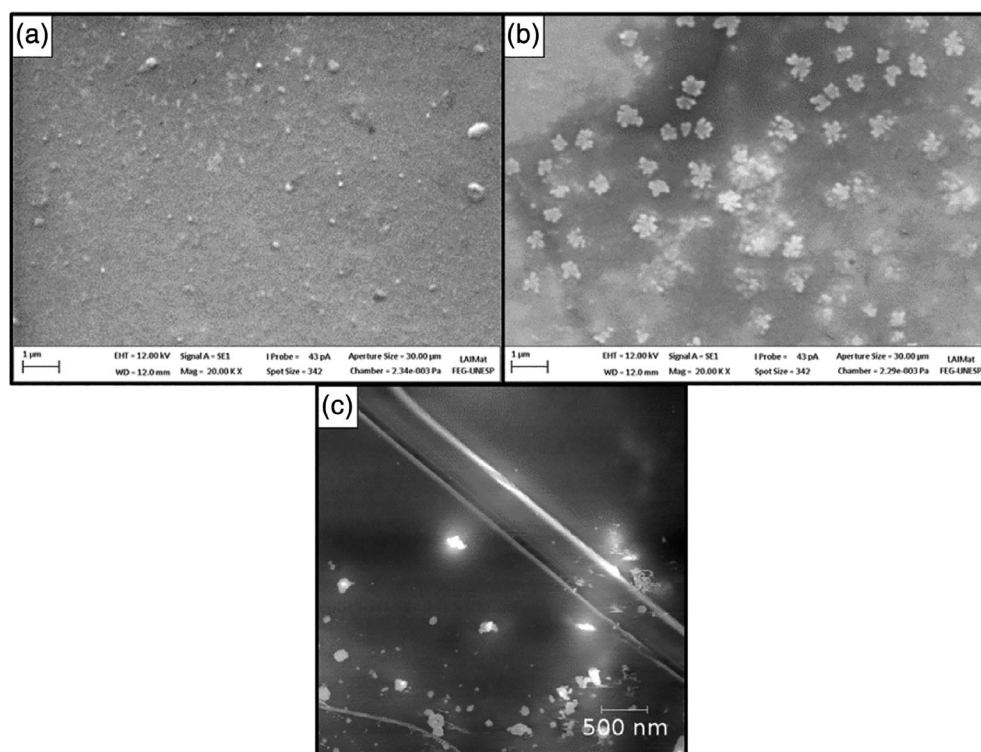
FIGURE 3 PEI/MWCNT film morphology (a) cross section and (b) front section view, (c) cross section view obtained through the AFM

**TABLE 1** Tensile results for PEI/CF and PEI/MWCNT/CF

	PEI/CF		PEI/MWCNT/CF	
	F^{tu} (MPa)	E (GPa)	F^{tu} (MPa)	E (GPa)
Room temperature (20°C)	611.8 ± 105.1	23.5 ± 2.3	642.7 ± 86.2	24.5 ± 1.1
Low temperature (−40°C)	392.7 ± 80.3	15.3 ± 1.9	395.5 ± 52.7	15.2 ± 1.4
High temperature (80°C)	421.1 ± 78.5	16.4 ± 2.1	428.5 ± 65.9	17.2 ± 1.7

the addition of MWCNT may be associated with several factors, such as their classification (single or multiple walls), source, purity, aspect ratio, concentration, orientation nature of the polymer matrix, and the dispersion of nanotubes. Previous studies[1,26] have shown that the addition of 1.0 wt% of carbon nanotubes, despite improving interfacial fiber–matrix adhesion and generating a strong synergistic effect between matrix and CNT, have not generated a significant increase in the tensile properties of the material.

It is worth mentioning the tensile strength of materials is directly affected by temperature, thus when the material is subjected to low temperature a reduction of 35 and 38% for PEI/CF and PEI/MWCNT/CF, respectively, was verified. Similar behavior was observed for the high-temperature condition with a reduction of 31 and 33% for PEI/CF and PEI/MWCNT/CF, respectively.

The reduction in tensile strength observed at low and high temperatures may be associated with thermal stress induced in the material, especially in the fiber/matrix interface, causing microcracks, and consequently, making easy the premature failure of the material.[50] Also, the softening of the polymer matrix modified the properties of composites, affecting the ability of the matrix to protect, unify and transfer the load to the fibers.[51,52]

In order to identify the possible mechanism of the fracture, fractographic analyses were carried out, as well as to evaluate the influence of the addition of MWCNT into the laminates. Figure 4 shows the micrographs of the fracture regions of the specimens subjected to tensile tests. Both micrographs illustrate the surface of the fractured fibers (red arrows) and the presence of the matrix adhered to the fibers (red circle), suggesting a good fiber/matrix interaction. On the other hand, for PEI/MWCNT/CF composite (Figure 4b), the polymeric matrix undergoes greater plastic deformation (yellow arrows) compared to the PEI/CF material (Figure 4a). This fact may be associated with the incorporation of MWCNTs into the composite that generated a greater energy absorption by the matrix before the final fracture. It is worth mentioning, in some cases the carbon nanotubes may exhibit high-plastic deformation.[28]
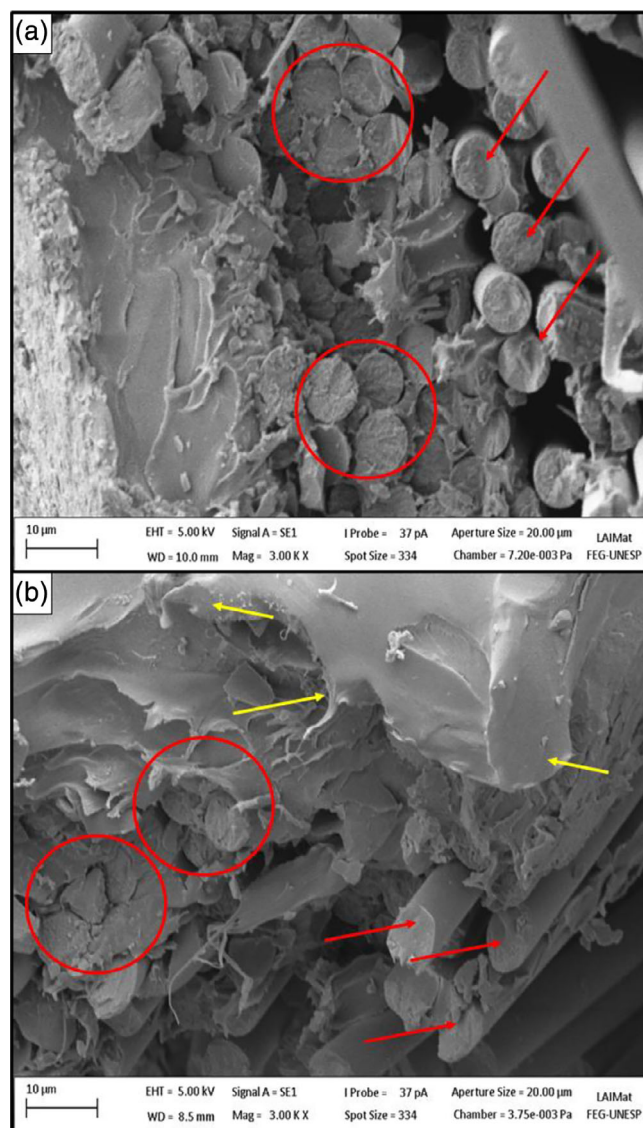
FIGURE 4 Micrograph of the fracture region for the laminates (a) PEI/CF and (b) PEI/MWCNT/CF subjected to tensile test [Color figure can be viewed at wileyonlinelibrary.com]

3.3 | Fatigue tests

Fatigue tests were carried to evaluate the effect of the addition of MWCNT on the fatigue strength of the prepared composites. The load used in this test was based on the load obtained by the specimens submitted to a tensile test. It is important to point out that there was an average

load reduction of 30% for the specimens tested at low- and high-temperature conditions. Therefore, the values obtained for PEI/CF and PEI/MWCNT/CF laminates decreased from 43.35 to 30.10 kN and from 39.71 to 27.30 kN, respectively. In the next step, fatigue tests were performed for the base laminate (PEI/CF) at room temperature at different loads (50, 55, 60, 65, 70, and 80% of the maximum tensile load) to determine the best condition to be used during the fatigue tests. The load of 65% (%Su) was defined to conduct the fatigue tests and a graph of %Su (maximum load) as the function of the number of cycles until failure is depicted in Figure 5. As can be seen, the data are very scattered, which may be associated with the heterogeneity and anisotropy of the composite material, defects, and imperfections introduced into the material during the processing step, and the environment of the test.[30] Also, it is quite common that the fatigue life for similar specimens or structures under the same stress level be significantly different.

To aid the interpretation, a statistical treatment is used, therefore, the most common treatments to study the fatigue life of composites materials are based on normal and Weibull distributions.[30,53,54] The normal distribution function was used in this work, in which the probability of the failure $P(x)$ was assigned to each result obtained. Therefore, the results of each condition were classified in increasing order of magnitude, with the classification numbers varying from $i = 1$ to $i = n$, and the statistical estimate for each $P(x)$ can be defined, as follows[30]:

$$P_f(x_i) = \frac{i - 0,3}{n + 0,4} \tag{6}$$

The classification, $P_f(x)$ and N_f (number of cycles to failure) for specimens submitted to fatigue tests at 65% of the maximum load is presented in Table 2, and the graph of $P_f(x)$ as the function of N_f are shown in Figure 6.

This Figure illustrates that at room temperature (20°C) the incorporation of MWCNT into the composite has not significantly influenced the fatigue life in the laminate (PEI/MWCNT/CF), resulting in only a small reduction in the fatigue life if compared to the control laminate (PEI/CF). This behavior may be associated with the agglomeration of MWCNT, which may have generated a higher concentration of tension in these regions promoting a premature failure. Meanwhile at elevated temperature condition (80°C) both processed laminates have shown an increase in fatigue life compared to materials at room temperature. The behavior observed in the literature[55–57] for composites when subjected to high temperatures is a reduction in fatigue life can be due to a nonlinear response resulting from the shear deformation of the polymeric matrix along the reinforcement fibers and there is also induced thermal stress that affects the matrix/fiber interface.[51,52] The pronouncement of this behavior at high temperatures is due to the viscoplastic nature of the polymeric matrix and these effects are most evident when it is close to the glass transition temperature.[55,57] However, the opposite behavior was observed in this work. The increase of the test temperature to 80°C
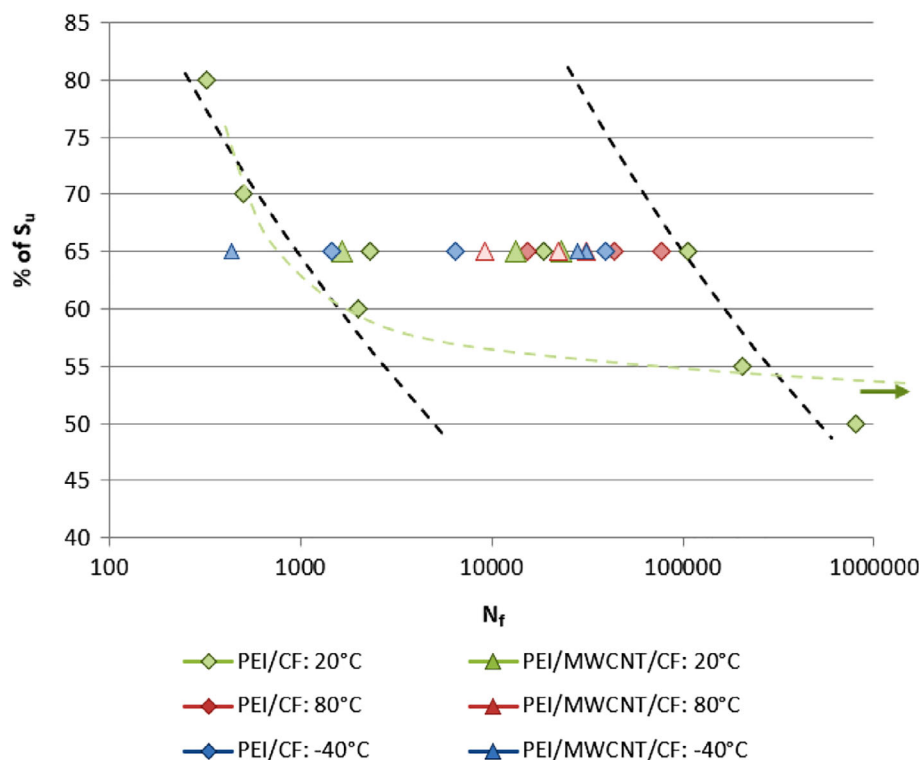
FIGURE 5 S–N curve obtained from the fatigue tests for PEI/CF and PEI/MWCNT/CF laminates [Color figure can be viewed at wileyonlinelibrary.com]

is far below from the glass transition temperature of the PEI (220°C), in other words, the high-temperature condition was not enough to induce thermal stress in the interface region and neither increase the shear deformation that can reduce the fatigue life. Also, this behavior may be associated to the test being performed with a load percentage of less than 65% since only one specimen of each

TABLE 2 Classification, $P_f(x)$ and N_f obtained from the normal distribution for PEI/CF and PEI/MWCNT/CF laminates

Laminate	Temperature (°C)	i	P_f	N_f
PEI/CF	−40	1	20.6	1,449
		2	50	6,456
		3	70.4	39,550
	20	1	20.7	2,303
		2	50	18,730
		3	70.5	106,761
	80	1	20.8	15,360
		2	50	44,125
		3	70.6	77,360
PEI/MWCNT/CF	−40	1	20.7	22,003
		2	50	28,317
		3	70.5	31,116
	20	1	20.8	1,643
		2	50	13,403
		3	70.6	23,213
	80	1	20.9	9,145
		2	50	22,433
		3	70.7	31,580

material was subjected to the static test to define the maximum load and perform the necessary corrections, in other words, it is not a representative condition of sampling. Despite this increase, the nanostructured laminate presented a lower fatigue resistance compared to the control sample (PEI/CF), which may be associated with the presence of MWCNT clusters as observed in the morphological analysis. At low-temperature condition (−40°C) it was observed the carbon nanotube laminate had a fatigue strength higher than the control sample. Also, in this low-temperature condition, the nanostructured laminate has shown a higher fatigue strength compared to PEI/MWCNT/CF at room temperature. Reducing the temperature made the polymer matrix to present a brittle behavior, thus reducing the fatigue life of the material. However, in the case of carbon nanotube laminates, it was found that the material did not weaken as the temperature decreased, that is, the presence of carbon nanotubes made the polymeric matrix maintain its ductile behavior even at extreme low-temperatures conditions.[2]

The fractographic analyses were classified according to temperature conditions studied in this work. The samples were obtained from the fracture region of each specimen and the analysis was conducted along with the thickness and width of the fracture region. It is important to point out that the presence of disordered fibers covering the surface made the observation of the fracture samples difficult. It was not possible to perform the SEM for PEI/CF sample at room temperature since the entire central area of the specimen was delaminated. In this particular case, the surface was observed by optical microscopy, as shown in Figure 7a. As can be seen, at the end of the test, the sample has shown total delamination
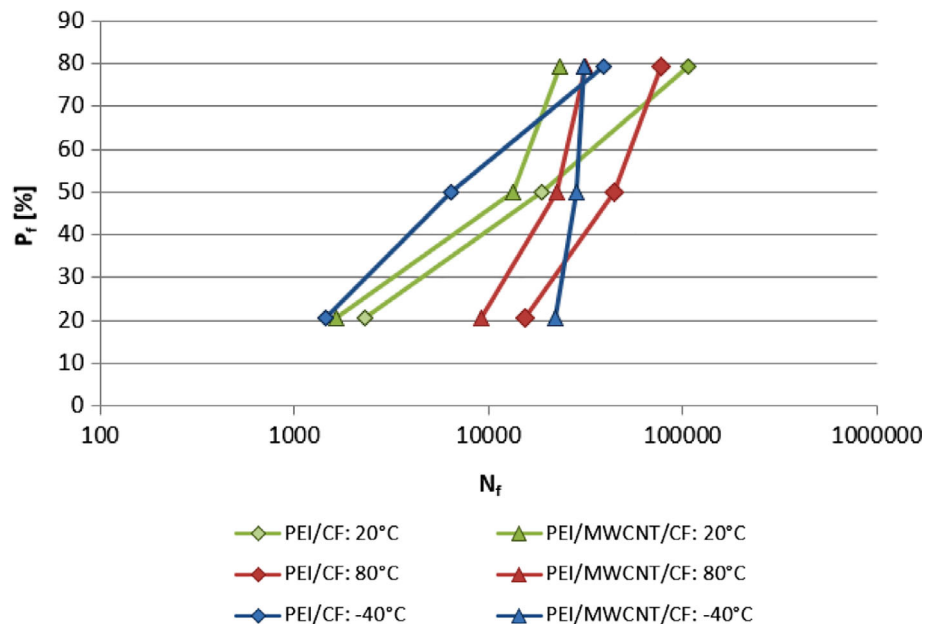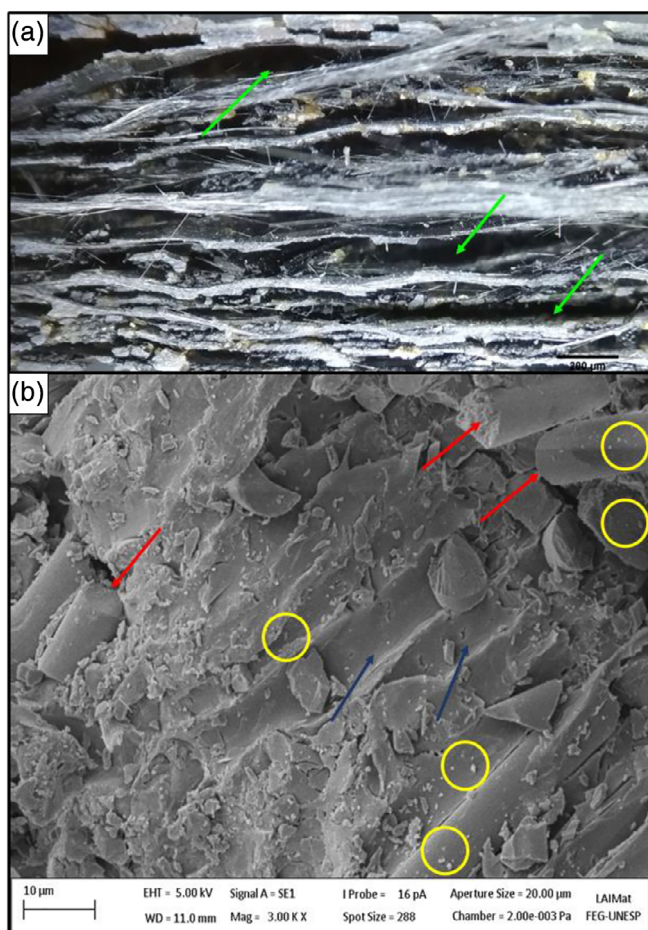

FIGURE 6 Graph of $P_f \times N_f$ for PEI/CF and PEI/MWCNT/CF laminates [Color figure can be viewed at wileyonlinelibrary.com]

(green arrows) of the layers, in which the fracture of the matrix occurred first, and the loose fibers in the region of the fracture held the specimen together. For PEI/MWCNT/CF sample (Figure 7b) fractured fibers (red arrows) and fiber imprint (blue arrows) were observed on the surface of the polymer matrix, as well as some clusters of nanotubes (yellows circles). As previously mentioned in this work, the agglomeration of MWCNT may have generated a higher stress concentration and caused premature failure compared to the PEI/CF laminate.[8,58]
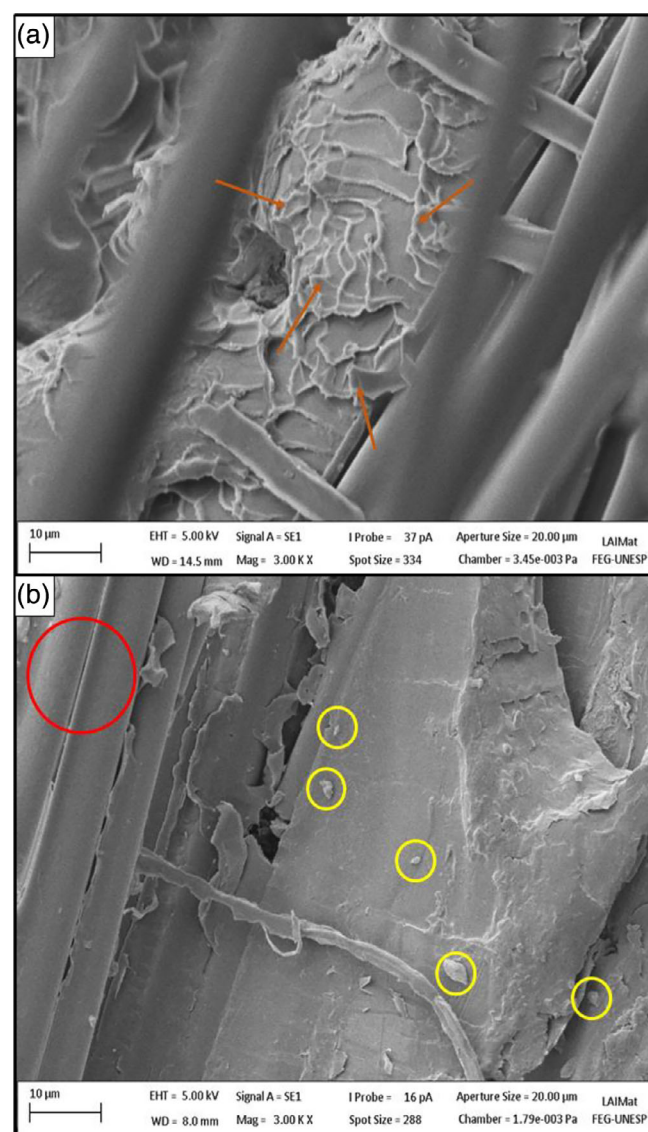
The images of the fracture regions for PEI/CF and PEI/MWCNT/CF composites subjected to the high-temperature condition fatigue test are shown in Figure 8a,b, respectively. As can be seen, for PEI/CF (Figure 8a), the carbon fibers covered the fracture region, revealing only a small area to be analyzed. Also, river marks (orange arrow) could be observed in this region, which can be explained by a progressive unification of several planes of neighboring fractures, such that planes are small and disordered during the failure of the

laminate.[59,60] For PEI/MWCNT/CF composite (Figure 8b) it can be seen that the carbon fibers were well adhered to the matrix (red circle), although there were fibers that were torn during the fracture of the specimen. Furthermore, small clusters of carbon nanotubes (yellow circle) can be visualized, which may have led to premature failure of the laminate.[31]

The fracture surfaces of the samples subjected to fatigue at the low-temperature condition are shown in Figure 9. For PEI/CF laminate (Figure 9a), there were a large number of river marks (orange arrow), which may have been generated by the impulses of the applied loads on the surface of the fibers during the opening of the sample. This behavior induced in this region an

FIGURE 7 Fatigue at room temperature: (a) fracture micrograph of PEI/CF laminate and (b) fracture micrograph of PEI/MWCNT/CF laminate [Color figure can be viewed at wileyonlinelibrary.com]

FIGURE 8 Fatigue at high temperature: (a) fracture micrograph of PEI/CF laminate and (b) fracture micrograph of PEI/MWCNT/CF laminate [Color figure can be viewed at wileyonlinelibrary.com]

interlaminar shear loading at the interface of composite material. PEI/MWCNT/CF laminate (Figure 9b) has shown the weft and warp both with good impregnation (red circles) in the polymer matrix, some matrix regions with fractures (purple arrow), and a few regions with river marks (orange arrows) compared to PEI/CF.

3.4 | Interlaminar shear strength

Figure 10 shows the absorbed moisture as a function of time (hours) for PEI/CF and PEI/MWCNT/FC laminates. As can be seen, both materials presented a Fickian behavior, which means the specimens absorbed water

quickly in the first 400 hr, reaching a state known as pseudo-equilibrium, after which this amount of water stays practically the same.[61]

Table 3 presents the results obtained from the ILSS and the CST tests. Firstly, for the samples without conditioning, it was verified the incorporation of MWCNT promoted an increase of 16% for ILSS and 58% for CST properties. According to Ashrafi[62] such improvements can be attributed to the high quality of the laminates obtained, that is, the low content of voids combined with the good interaction between the carbon nanotubes and PEI made difficult the growth of the crack within the matrix. Furthermore, the increase of shear properties may be associated with the increase of the surface roughness of the carbon fibers due to the incorporation of the nanoparticles. The strong interfacial adhesion of the PEI/MWCNT/CF composite associated with the increased roughness may be responsible for a mechanical interlocking, which would contribute to an increase of the coefficient of friction, and consequently, an increase in the shear properties.[63]

It is important to mention that both aging conditions studied in this work promoted the degradation of shear properties of the composites. The hygrothermal aging led to a decrease of about 78% (PEI/CF) and 85% (PEI/MWCNT/CF) for samples tested by ILSS. The same tendency of decreasing was found in CST showing a reduction of 12% (PEI/CF) and 35% (PEI/MWCNT/CF). The absorbed water remained within the laminate and tends to penetrate the polymer matrix over time by the concentration gradient, especially in the fiber–matrix interface, promoting the matrix degradation. In addition, the continuous exposure of humidity into the laminates
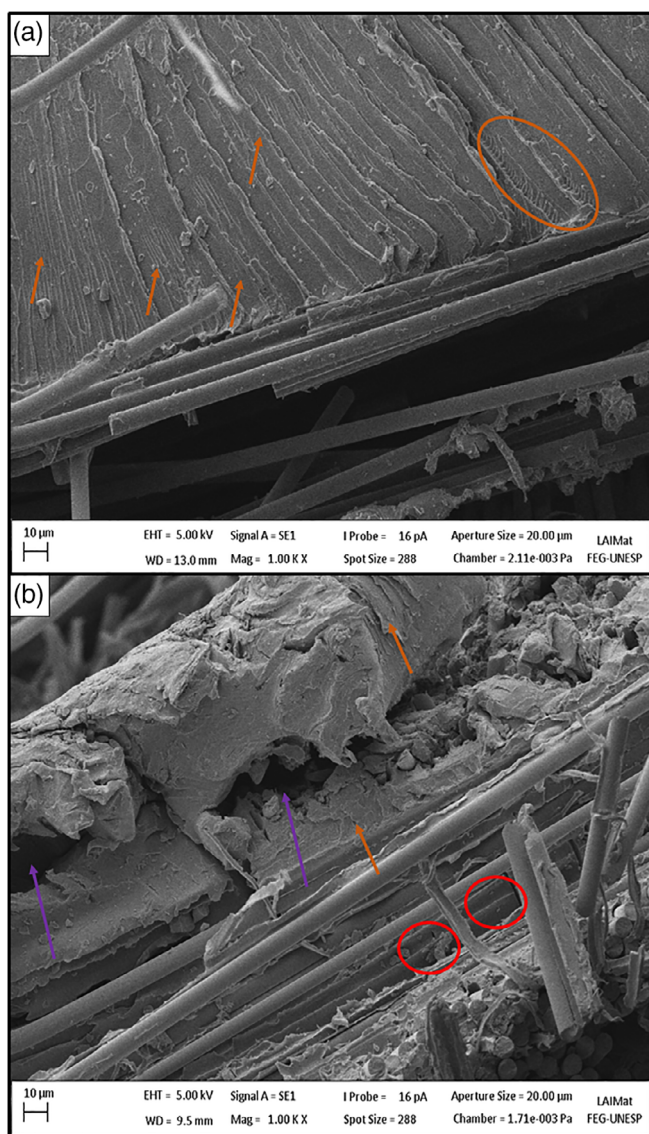
FIGURE 9 Fatigue at low temperature: (a) fracture micrograph of PEI/CF laminate and (b) fracture micrograph of PEI/MWCNT/CF laminate [Color figure can be viewed at wileyonlinelibrary.com]
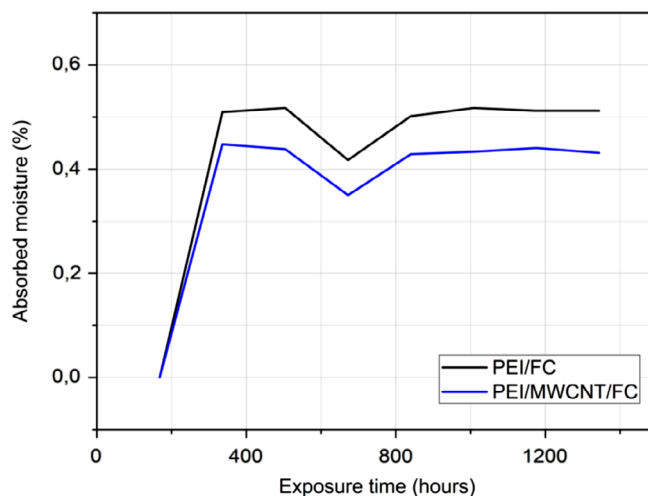
FIGURE 10 Humidity absorbed during hygrothermal conditioning [Color figure can be viewed at wileyonlinelibrary.com]

initiated the relaxation process of the polymer chain, as long as the temperature may have introduced thermal stress, resulting in a deterioration of the properties of the composite.[61,64,65]

The UV radiation with condensation promoted almost the same behavior compared to hygrothermal conditioning. As can be seen, ILSS properties decreased around 73% (PEI/CF) and 87% (PEI/MWCNT/CF), and the same tendency was observed in CST. However, In contrast to hygrothermal aging, the UV radiation and condensation tends to act in the direction of the failure by photooxidation. In this case, the failures are associated

TABLE 3 Results obtained from the ILSS and CST tests

|	ILSS (MPa)		CST (MPa)	
	PEI/CF	PEI/MWCNT/CF	PEI/CF	PEI/MWCNT/CF
Without conditioning	86.27 ± 6.89	100.48 ± 6.99	30.33 ± 7.93	35.29 ± 9.68
UV radiation (with condensation)	22.93 ± 1.63	13.38 ± 1.46	24.88 ± 2.32	25.50 ± 2.35
Hygrothermal	19.03 ± 1.64	15.55 ± 2.34	26.68 ± 8.23	23.03 ± 6.41
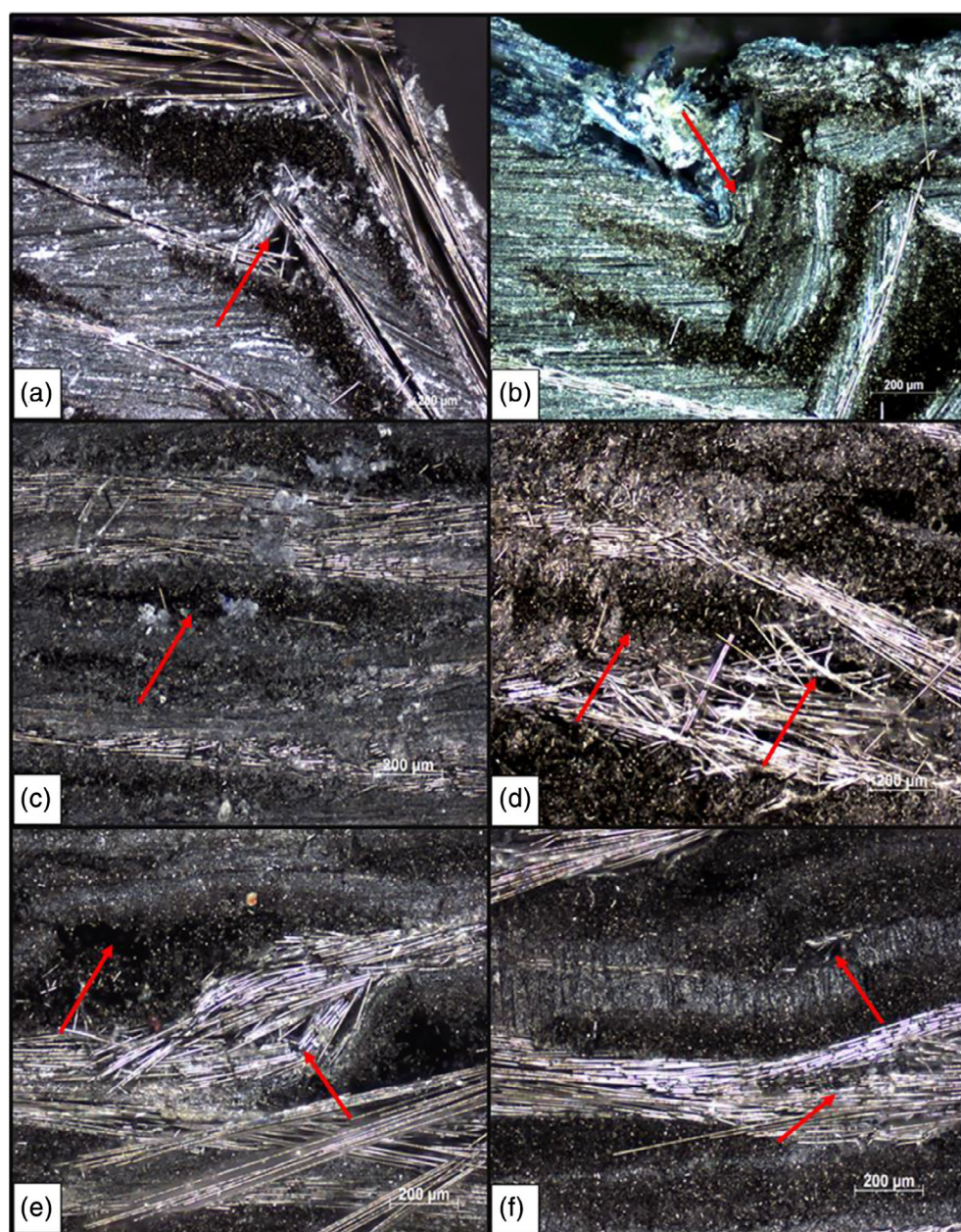
FIGURE 11 The micrographs for fracture surface of the specimens submitted to ILSS test: (a) PEI/CF, (b) PEI/MWCNT/CF without conditioning, (c) PEI/CF, (d) PEI/MWCNT/CF hygrothermal, (e) PEI/CF, and (f) PEI/MWCNT/CF UV radiation [Color figure can be viewed at wileyonlinelibrary.com]

with reactions and damages that promoted changes in the polymeric matrix, such as oxidation, chain scission, and crosslinking.[16] Chain scission is associated with the breaking of the molecular chain that results in weak bonds in the polymer chain.[17] On the other hand, crosslinking restricts the molecular mobility and may lead to excessive brittleness of the matrix, leading to microcracks on the surface of the matrix, and consequently, decreasing the interlaminar fracture strength of the material. Besides, the UV and water condensation acted synergistically into the laminates, causing the formation of microcracks due to water absorption and swelling that was accelerated by UV degradation.[40,66]

After the mechanical tests, the fracture surface was analyzed by optical microscopy and the images are presented in Figures 11 and 12. The fracture on both images is indicated by red arrows. As can be seen in Figure 11, both laminates at the three different temperature conditions submitted to the ILSS test presented the fracture in the central region, that is, at the place of loading application. It was also observed that the material without conditioning (Figure 11a,b), firstly presented an interlaminar fracture that propagated to translaminar fracture, and subsequently, the specimens were in the V shape. The laminates submitted to both conditioning (Figure 11c–f) have shown a weakening of the fiber–matrix interface, showing the fracture in the interlaminar region. In addition, the hygrothermal and UV radiation with condensation promoted the degradation of the laminates, and the images (Figure 12) for the specimens submitted to CST have shown that both composites presented interlaminar
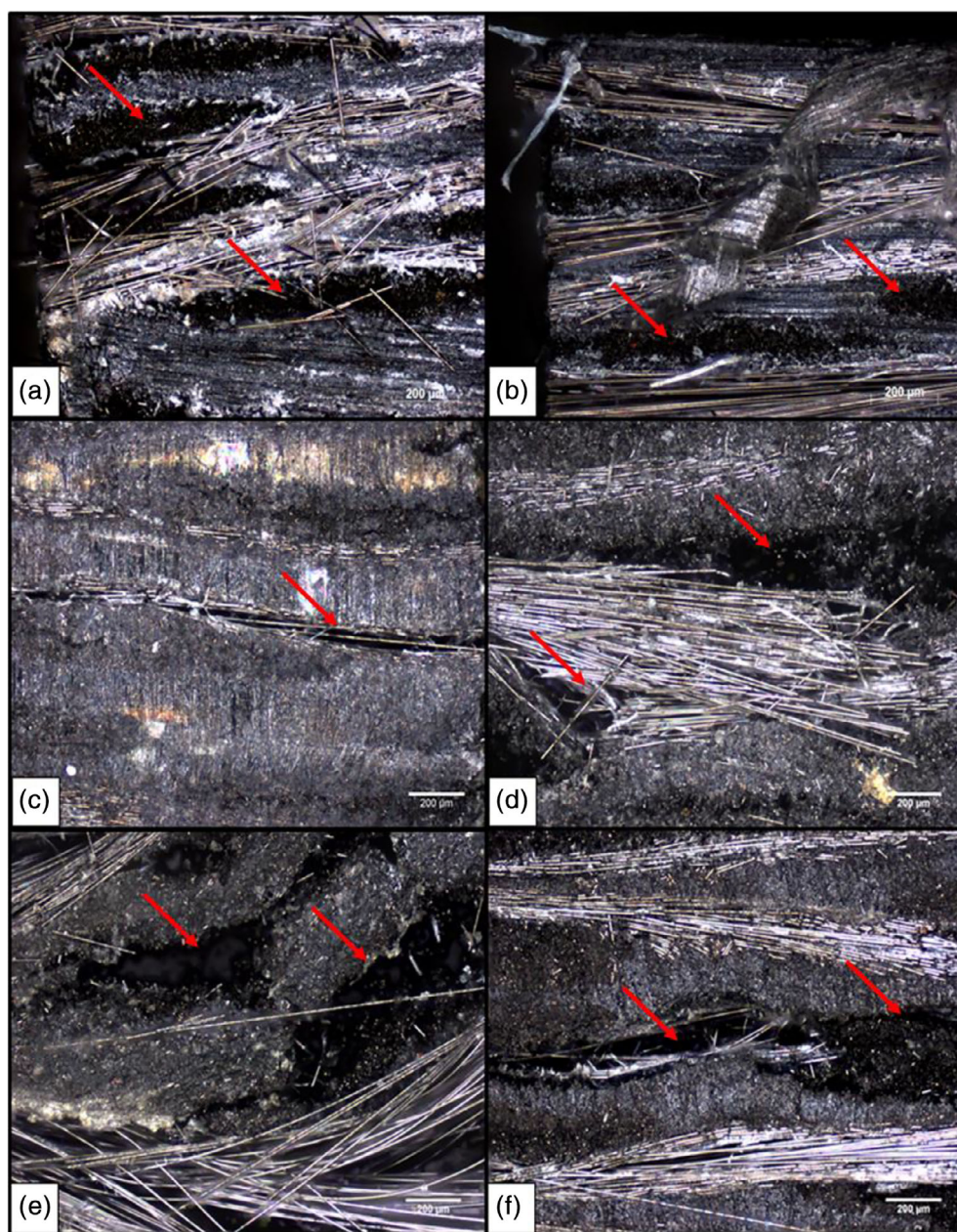
FIGURE 12 The micrographs for fracture surface of the specimens submitted to CST test: (a) PEI/CF, (b) PEI/MWCNT/CF without conditioning, (c) PEI/CF, (d) PEI/MWCNT/CF hygrothermal, (e) PEI/CF, and (f) PEI/MWCNT/CF UV radiation [Color figure can be viewed at wileyonlinelibrary.com]

fracture. This behavior was the same compared to the ILSS test, which means the laminates submitted to both conditioning described in this work have shown a more fragile fracture compared to non-conditioning laminates.

4 | CONCLUSIONS

The addition of MWCNTs promoted improvements in the mechanical behavior of PEI/CF laminate, as can be seen in tensile, ILSS and CST tests. Also, the fatigue life of the composites was dependent on temperature. However, a greater contribution was observed to laminates submitted to tests, in which the loading was shear. From the tensile test, it was found that the incorporation of MWCNT promoted a 5% increase in tensile strength and 2% in Young's modulus of the material, which is not significant considering the standard deviation. Fatigue results revealed the addition of MWCNT has not significantly influenced the fatigue life of the laminates at room and high temperature. However, at a sub-ambient temperature, the MWCNT addition favored and generated an improvement in the fatigue strength of the composite. For the ILSS and CST, it was found improvements around 16 and 58%, respectively, confirming a larger contribution of MWCNT to shear stresses. However, laminates submitted to hygrothermal aging and UV radiation with condensation suffered a degradation of their properties, showing a reduction of around 80 and 30% for the ILSS and CST tests. Fractographic analyses have shown the difference between the fracture aspects and it was confirmed that the fracture for the nanostructured composite was more ductile.

ORCID
Luis F. P. Santos https://orcid.org/0000-0002-5089-1089

REFERENCES
[1] A. M. Díez-Pascual, M. Naffakh, C. Marco, M. A. Gómez-Fatou, G. Ellis, *J. Curr. Opin. Solid State Mater. Sci.* **2014**, *18*, 62.
[2] P. Coronado, A. Argüelles, J. Viña, I. Viña, *Compos. Struct.* **2014**, *112*, 188.
[3] I. González, J. I. Eguiazábal, *Compos. A Appl. Sci. Manuf.* **2013**, *53*, 176.
[4] E. S. Lee, Y. K. Lim, Y. S. Chun, B. Y. Wang, D. S. Lim, *Carbon N. Y.* **2017**, *118*, 650.
[5] L. Tzounis, M. Hegde, M. Liebscher, T. Dingemans, P. Pötschke, A. S. Paipetis, N. E. Zafeiropoulos, M. Stamm, *Compos. Sci. Technol.* **2018**, *156*, 158.
[6] A. M. Díez-Pascual, M. Naffakh, C. Marco, G. Ellis, *Compos. A Appl. Sci. Manuf.* **2012**, *43*, 603.
[7] S. Iijima, *Nature* **1991**, *354*, 56.
[8] G. Mittal, V. Dhand, K. Y. Rhee, S.-J. Park, W. R. Lee, *J. Ind. Eng. Chem.* **2015**, *21*, 11.
[9] A. V. Desai, M. A. Haque, *Thin-Walled Struct.* **2005**, *43*, 1787.
[10] L. Peponi, D. Puglia, L. Torre, L. Valentini, J. M. Kenny, *Mater. Sci. Eng. R Rep.* **2014**, *85*, 1.
[11] B. Ribeiro, E. C. Botelho, M. L. Costa, C. F. Bandeira, *Polímeros* **2017**, *27*, 247.
[12] J. A. Rojas, L. A. Ardila-Rodríguez, M. F. Diniz, M. Gonçalves, B. Ribeiro, M. C. Rezende, *Mater. Des.* **2019**, *166*, 107612.
[13] A. M. Vorobei, O. I. Pokrovskiy, K. B. Ustinovich, O. O. Parenago, S. V. Savilov, V. V. Lunin, V. M. Novotortsev, *Polymer* **2016**, *95*, 77.
[14] C. Pramanik, D. Nepal, M. Nathanson, J. R. Gissinger, A. Garley, R. J. Berry, A. Davijani, S. Kumar, H. Heinz, *Compos. Sci. Technol.* **2018**, *166*, 86.
[15] M. Karimi, N. Solati, M. Amiri, H. Mirshekari, E. Mohamed, M. Taheri, M. Hashemkhani, A. Saeidi, M. A. Estiar, P. Kiani, A. Ghasemi, S. M. M. Basri, A. R. Aref, M. R. Hamblin, *Expert Opin. Drug Deliv.* **2015**, *12*, 1071.
[16] K. Yang, M. Gu, Y. Guo, X. Pan, G. Mu, *Carbon N. Y.* **2009**, *47*, 1723.
[17] W. Francisco, F. V. Ferreira, E. V. Ferreira, L. de Simone Cividanes, A. dos Reis Coutinho, G. Patrocínio Thim, *J. Aerosp. Technol. Manag.* **2015**, *7*, 289.
[18] M. Kadlec, L. Nováková, I. Mlch, L. Guadagno, *Compos. Science Techno.* **2016**, *131*, 32.
[19] N. Dubary, G. Taconet, C. Bouvet, B. Vieille, *Compos. Struct.* **2017**, *168*, 663.
[20] E. Schuhler, A. Coppalle, B. Vieille, J. Yon, Y. Carpier, *Polym. Degrad. Stab.* **2018**, *152*, 105.
[21] X. Gabrion, V. Placet, F. Trivaudey, L. Boubakar, *Compos. B Eng.* **2016**, *95*, 386.
[22] G. Szebényi, B. Magyar, T. Iványicki, *Polym. Test.* **2017**, *63*, 307.
[23] A. Yudhanto, H. Wafai, G. Lubineau, R. Yaldiz, N. Verghese, *Compos. Struct.* **2018**, *186*, 324.
[24] M. K. Pitchan, S. Bhowmik, M. Balachandran, M. Abraham, *Mater. Des.* **2017**, *127*, 193.
[25] H. Wang, S. Zhang, M. Zhu, G. Sui, X. Yang, *J. Electroanal. Chem.* **2018**, *808*, 303.
[26] M. Tunckol, E. Z. Hernandez, J. R. Sarasua, J. Durand, P. Serp, *Eur. Polym. J.* **2013**, *49*, 3770.
[27] M. May, S. R. Hallett, *Int. J. Fatigue* **2016**, *87*, 59.
[28] L. P. Borrego, J. D. M. Costa, J. A. M. Ferreira, H. Silva, *Compos. B* **2014**, *62*, 65.
[29] R. Shrestha, J. Simsiriwong, N. Shamsaei, *Polym. Test.* **2016**, *56*, 99.
[30] V. Damodaran, A. G. Castellanos, M. Milostan, P. Prabhakar, *Mater. Des.* **2018**, *157*, 60.
[31] H. Chen, J. Wang, A. Ni, A. Ding, S. Li, X. Han, *Compos. Struct.* **2018**, *208*, 498.
[32] S. Mortazavian, A. Fatemi, *Int. J. Fatigue* **2017**, *102*, 171.

[33] S. K. Bhaumik, M. Sujata, M. A. Venkataswamy, *Eng. Fail. Anal.* **2008**, *15*, 675.

[34] G. Mustafa, C. Crawford, A. Suleman, *Compos. Struct.* **2016**, *151*, 149.

[35] P. Alam, D. Mamalis, C. Robert, C. Floreani, Ó. B. CM, *Compos. B Eng.* **2019**, *166*, 555.

[36] F. Sacchetti, W. J. B. Grouve, L. L. Warnet, I. Fernandez Villegas, *Polym. Test.* **2018**, *66*, 13.

[37] V. K. Srivastava, T. Gries, D. Veit, T. Quadflieg, B. Mohr, M. Kolloch, *Eng. Fract. Mech.* **2017**, *180*, 73.

[38] N. H. Nash, T. M. Young, W. F. Stanley, *Compos. A Appl. Sci. Manuf.* **2016**, *81*, 111.

[39] S. Menbari, A. Ashori, H. Rahmani, R. Bahrami, *Polym. Test.* **2016**, *54*, 186.

[40] N. L. Batista, M. C. Rezende, E. C. Botelho, *Polym. Degrad. Stab.* **2018**, *153*, 255.

[41] I. Panaitescu, T. Koch, V. M. Archodoulaki, *Polym. Test.* **2019**, *74*, 245.

[42] A. Boubakri, N. Guermazi, K. Elleuch, H. F. Ayedi, *Mater. Sci. Eng. A* **2010**, *527*, 1649.

[43] L. Mansouri, A. Djebbar, S. Khatir, M. Abdel Wahab, *Compos. Struct.* **2019**, *207*, 816.

[44] M. Eftekhari, A. Fatemi, *Polym. Test.* **2016**, *51*, 151.

[45] F. Dalcanale, J. Grossenbacher, G. Blugan, M. R. Gullo, J. Brugger, H. Tevaearai, T. Graule, J. Kuebler, *J. Colloid Interface Sci.* **2016**, *470*, 123.

[46] T. Liu, Y. Tong, W. De Zhang, *Compos. Sci. Technol.* **2007**, *67*, 406.

[47] L. F. P. Santos, B. Ribeiro, L. R. O. Hein, E. C. Botelho, M. L. Costa, *Mater. Res. Express* **2017**, *4*, 075302.

[48] K. Schneider, B. Lauke, W. Beckert, *Appl. Compos. Mater.* **2001**, *8*, 43.

[49] Y. Y. Liang, J. Z. Xu, X. Y. Liu, G. J. Zhong, Z. M. Li, *Polymer (Guildf)* **2013**, *54*, 6479.

[50] K. K. Mahato, K. Dutta, B. C. Ray, *J. Appl. Polym. Sci.* **2017**, *134*, 44715.

[51] S. Cao, Z. Wu, X. Wang, *J. Compos. Mater.* **2009**, *43*, 315.

[52] F. Nardone, M. Di Ludovico, Y. De Caso, F. J. Basalo, A. Prota, A. Nanni, *Compos. B Eng.* **2012**, *43*, 1468.

[53] A. Tuğrul Seyhan, *Polym. Polym. Compos.* **2011**, *19*, 717.

[54] D. Djeghader, B. Redjel, *Adv. Compos. Lett.* **2019**, *28*, 096369351985383.

[55] R. Růžek, M. Kadlec, L. Petrusová, *Int. J. Fatigue* **2018**, *113*, 253.

[56] M. Kawai, S. Yajima, Y. Kawase, A. Hachinohe, *Trans. Jpn. Soc. Mech. Eng. A* **1999**, *65*, 791.

[57] B. Vieille, J. Aucher, L. Taleb, *Mater. Sci. Eng. A* **2009**, *517*, 51.

[58] V. Romanov, S. V. Lomov, I. Verpoest, L. Gorbatikh, *Compos. Sci. Technol.* **2015**, *114*, 79.

[59] L. A. L. Franco, M. L. A. Graça, F. S. Silva, *Mater. Sci. Eng. A* **2008**, *488*, 505.

[60] T. Jollivet, E. Greenhalgh, *Procedia Eng.* **2015**, *133*, 171.

[61] L. Liu, Z. Zhao, W. Chen, C. Shuang, G. Luo, *Compos. Struct.* **2018**, *204*, 645.

[62] B. Ashrafi, A. M. Díez-Pascual, L. Johnson, M. Genest, S. Hind, Y. Martinez-Rubi, J. M. González-Domínguez, M. Teresa Martínez, B. Simard, M. A. Gómez-Fatou, A. Johnston, *Compos. A Appl. Sci. Manuf.* **2012**, *43*, 1267.

[63] J. Li, T. Bai, *Polym. Plast. Technol. Eng.* **2011**, *50*, 1393.

[64] E. Faguaga, C. J. Pérez, N. Villarreal, E. S. Rodriguez, V. Alvarez, *Mater. Des.* **2012**, *36*, 609.

[65] S. Sethi, B. C. Ray, *Adv. Colloid Interface Sci.* **2015**, *217*, 43.

[66] M. C. M. de Faria, F. C. Appezzato, M. L. Costa, P. C. de Oliveira, E. C. Botelho, *J. Reinf. Plast. Compos.* **2011**, *30*, 1729.

[67] B. Ribeiro, L. F. P. Santos, A. L. Santos, M. L. Costa, E. C. Botelho, *J. Thermoplast. Compos. Mater.* **2019**, *32*, 62.